Elastic-plastic Behaviour of Perforated Aluminium under Tension and Compression

A. Öchsner, W. Winter, G. Kuhn

The elastic-plastic behaviour of perforated aluminium sheets is examined in relation to the relative density. A compression device, which permits a changeable support of the specimens, was designed for that purpose. The gained results are discussed in the context of a modified Voigt-Reuss mixing rule and are compared with results from tensile tests. The experiments are simulated by means of finite element calculations, expanded on smaller relative densities and the influence of the boundary conditions at the ends of the specimens on the results is examined. Finally, the initial yielding on the microscale is examined and compared to macroscopically determined values.

1 Introduction

Cellular metals, eg. aluminium foams, exhibit particular properties and are currently being considered for use in lightweight structures or passive safety devices. Suggested applications can be found e.g. in Ashby et al. (2000). The mechanical properties of cellular materials, in particular their resistance to plastic deformation, the evolution of damage, and fracture, are determined by the microstructure (Gibson et al., 1997). Experiments on metallic foams as well as on biological materials, e.g. trabecular bone, show that the experimentally determined characteristics can be related to the relative density and that the characteristics show a significant spread due to the heterogeneous structure (cf. Figure 1, a-b) of the materials (cf. Öchsner et al., 2000).
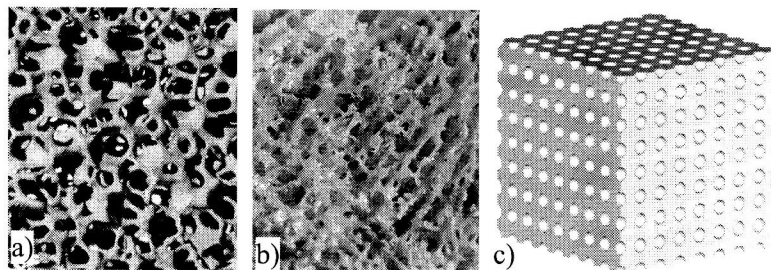

Figure 1: Cellular Materials, a) Open Cell Al-Foam b) Trabecular Bone c) Perforated Metal

Furthermore, the experimental values deviate clearly from theoretical characteristics, that were derived with the aid of idealized models based on regular unit cells (cf. Kuhn et al., 2000). Common models for the elastic and inelastic characteristics of open-cell and closed-cell foams were derived by Gibson and Ashby (1982) by means of cubic cell models. Another approach (cf. Hashin, 1963) is based on the use of variational principles in order to bound the strain energy and thus also the effective elastic characteristics to special shape of inclusions (e.g. spherical or ellipsoidal). Multiaxial stress-states are difficult to realize with experiments. Therefore, perforated aluminium plates were used for fundamental studies of the mechanical behaviour of cellular metals. Although the relative density of metallic foam is smaller than 0.1, the plates with a relative density larger than 0.5 were used for basic studies, since very simple homogeneous specimens for all types of experiments can be produced on that basis. Uniaxial tension and/or compression tests are usually conducted on the cellular materials and the plastic behaviour is characterized by means of the hardening curves. The continuum-mechanical characteristics are defined by means of the macro-behaviour.

Perforated plates were experimentally investigated for the reason that they are used in the construction of tubular heat exchangers, reactor diagrids, boiler drums and some aerospace and civil engineering structures. Apart from the elastic characteristics of flat specimens under simple tensile loading (cf.

Bailey et al., 1960; Duncan et al., 1963; Meguid et al., 1996), the plastic behaviour was also examined in particular by means of perforated tubes (cf. Litewka, 1980; Litewka, 1981).

No experimental data for flat specimens under compression load is available in the literature. The elastic-plastic behaviour of perforated flat specimens under compression with respect to the relative density is presented in this paper for the very first time.

2 Specimen Design and Apparatus

Different parameters can be used for the geometrical description of perforated flat specimens with regular (square) penetration pattern (cf. Litewka, 1980; Markov, 1981). The ligament efficiency (cf. Figure 2)

$$\mu = \frac{c}{t} \tag{1}$$

where c is the minimum ligament section and t is the perforation pitch and/or the relative plate area (ratio of the solid area to the unperforated initial area), that just corresponds to the relative density

$$\phi_S = \frac{\rho^*}{\rho_S} = 1 - \frac{\pi}{4}(1 - \mu)^2 \tag{2}$$

where ρ^* is the average density of the plate and ρ_S the density of the solid part are suitable descriptions in the context of cellular materials.
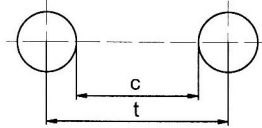

Figure 2: Geometrical Description of Perforated Plates

The specimens were machined from 2 mm thick plates of aluminium alloy AlCuMg1. Different relative densities could be achieved by modification of the hole spacing (cf. Table 1). The holes had a constant diameter of 1.5 mm and were drilled by means of a precise CNC-machine.

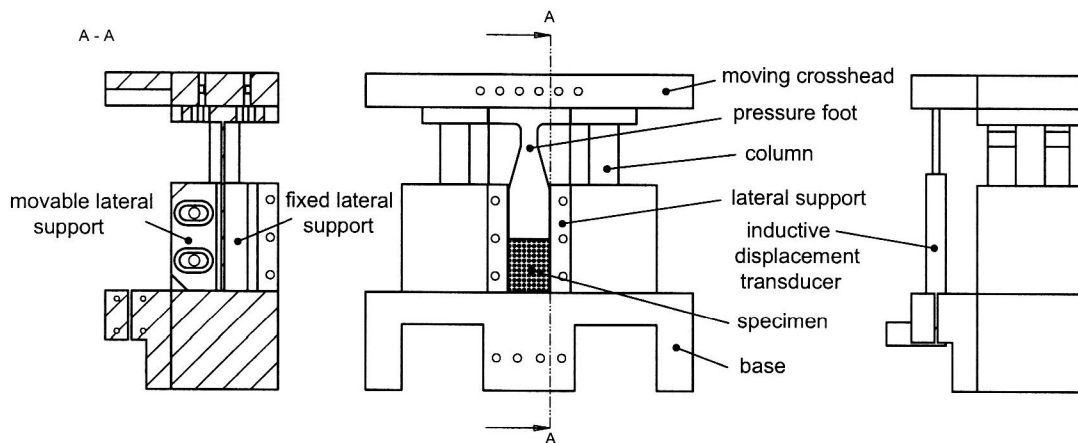| Ligament Efficiency μ	1	0.7	0.5	0.4	0.3
Relative Density ρ^*/ρ_S	1	0.9293	0.8037	0.7173	0.6152

Table 1: Realized Geometry

Figure 3: Schematic Representation of the Compression Testing Device

The design of the compression testing device needs to intentionally inhibit some failure modes such as column buckling and end brooming. Therefore, the testing device consits of a moving crosshead that is guided by a pair of columns and a supported test section (cf. Figure 3). The guidance is realized

with lateral fixed and movable supports. Thus the tolerance remains adjustable between specimen and support. This allows that also specimens with different thickness can be tested if the pressure foot is exchanged. Load is introduced into the test section through end-loading.

The test is performed in the following manner: After precise placing the specimen in the test fixture and the right setting of the supports, a compressive load is applied torque-free to the end of the fixture in a standard testing machine and transferred from the crosshead through a pressure foot to the specimen. The displacement is recorded by means of an inductive displacement transducer.

The compression fixture was installed in a universal electro magnetic testing machine (SCHENCK) with a capacity of 100 kN and an appropriate load cell (cf. Figure 4).
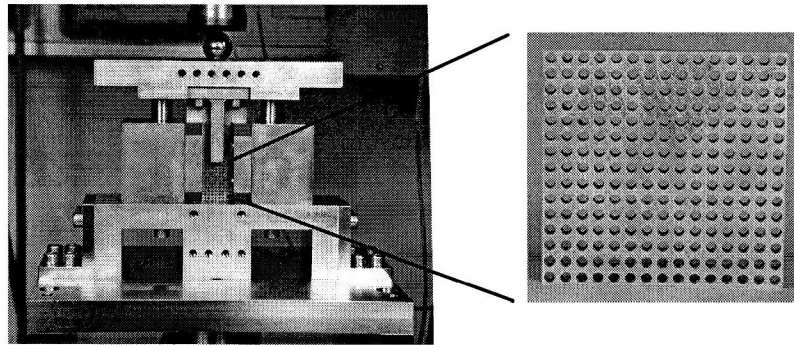

Figure 4: Installed Compression Fixture and Used Specimen

3 Test Procedure and Results

The specimens were loaded elongation controlled (elongation speed 1 mm/min.) up to a total value of 2 mm and the load-elongation curves were recorded. The stress strain-diagrams (cf. Figure 5) were calculated from the obtained data. In this case, the engineering stress is computed by dividing the load by the original cross-sectional area. From these diagrams the Young's modulus was obtained as the gradient of the linear section of the diagram and the yield point was definied as a stress corresponding to the permanent strain equal to 0.2 %. The elastic-plastic properties of the unperforated material were analysed in Öchsner et al. (2000) and the Young's modulus was $E_S = 72700$ MPa and the uniaxial yield stress (0.2 % offset) was equal to $Y_S = 273$ MPa.
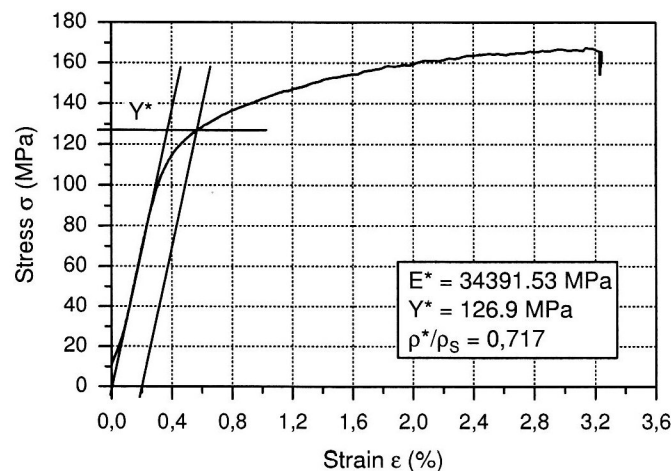

Figure 5: Experimental Stress-Strain-Diagram

The results of the compression tests are evaluated by means of modified Voigt-Reuss mixing rules for cellular materials (Öchsner et al., 2000), where only the knowledge of the volume fractions of the phases is required without the need to know the spatial distribution or the shape of the phases. This formulation provides for a simple transfer of obtained data on materials with a complex microstructure (e.g. aluminium foams). This simple mechanical model for two-phase materials is realized with a parallel- and/or series connections of springs. The basis of the model is a Voigt-partition, at which the two phases are

103

connected in parallel (isostrain state) and a Reuss-partition that results from series connection (isostress state) of the two phases. A parallel connection of these two branches leads to a hybridized Voigt/Reuss mixing rule, in which the volume fraction of the Voigt partition is α and that of the Reuss partition $(1 - \alpha)$ respectively (cf. Figure 6).
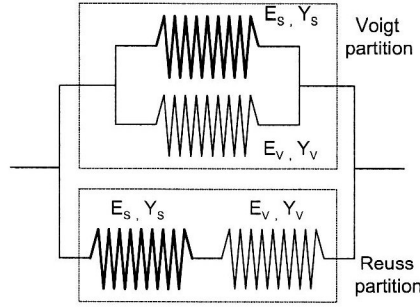

Figure 6: Hybridized Voigt/Reuss Mixing Rule

The effective stiffness of the mixture E^* in relation to the relative density ϕ_S is formulated as

$$E^* = \alpha \cdot E^*_{Voigt} + (1-\alpha) \cdot E^*_{Reuss} = \alpha \cdot [\phi_S \cdot E_S + (1 - \phi_S) \cdot E_V] + (1-\alpha) \cdot \left[\frac{\phi_S}{E_S} + \frac{1 - \phi_S}{E_V} \right]^{-1} \tag{3}$$

where E_S is the stiffness of the solid and E_V the stiffness of the void phase. Although the void phase does not contribute to the stiffness of the mixture, a stiffness ratio of $E_V/E_S = 10^{-6}$ needs to be maintained to avoid singularity of the hybrid rule (Swan et al., 1997). Accordingly, the effective yield stress Y^* of the mixture can be calculated in relation to the yield stress of the solid Y_S and the yield stress of the void phase Y_V as:

$$Y^* = \alpha \cdot Y^*_{Voigt} + (1-\alpha) \cdot Y^*_{Reuss} = \alpha \cdot [\phi_S \cdot Y_S + (1 - \phi_S) \cdot Y_V] + (1-\alpha) \cdot \begin{cases} Y_V & 0 \leq \phi_S < 1 \\ Y_S & \phi_S = 1 \end{cases} \tag{4}$$

In the mixing rules a varying fractional parameter $\alpha = \alpha(\phi_s)$ has to be used for the adequate graphic representation of experimental results:

$$\alpha = \begin{cases} \alpha_0 & 0 \leq \phi_s \leq \phi_{break} \\ \alpha_0 + (1 - \alpha_0) \cdot \dfrac{(\phi_s - \phi_{break})^2}{(1 - \phi_{break})^2} & \phi_{break} < \phi_S \leq 1 \end{cases} \tag{5}$$

In accordance with the continuum damage mechanics, α can be regarded as a supplementary parameter which is supposed to register the influence of the complex microstructure of cellular materials on the macro-behaviour. In this case, a detailed modeling of the microstructure is not necessary. The parameter α has to be determined experimentally for a representative volume.
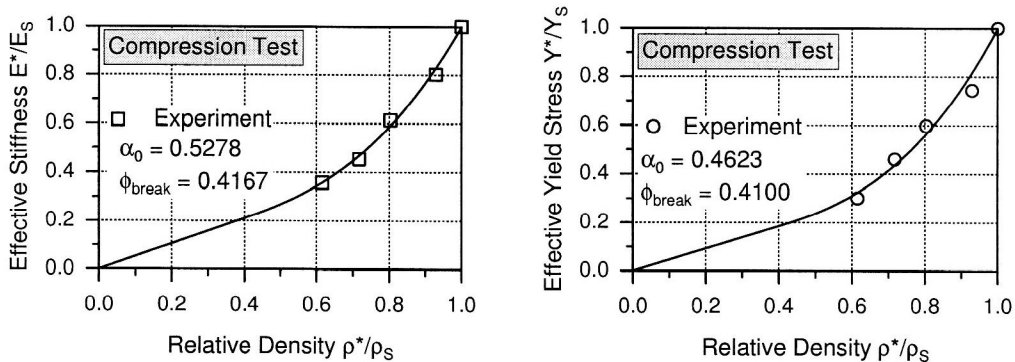

Figure 7: Results of the Compression Tests

To fit the proposed functions to a set of $N + 1$ experimental data points (ϕ_{Si}, E_i^*) or (ϕ_{Si}, Y_i^*) the two parameters α_0 and ϕ_{break} are judged on the basis to minimize the sum of the squared differences between the input data points and the function values, evaluated at the same locations ('chisquare'):

$$\sum_{i=0}^{N} [E^*(\phi_{Si}, \alpha_0, \phi_{break}) - E_i^*]^2 \overset{!}{=} \min. \tag{6}$$

The same procedure was also used for the approximation of the parameters for the yield stress.

The results for the effective Young's modulus and the effective yield stress are given in Figure 7. It can be seen that the presented mixing rule show good agreement with the experimental results.

4 Comparison with Tensile Tests

The specimens used in the uniaxial tensile test (cf. Figure 8) were flat with an overall length of 193.4 mm and a thickness of 2 mm. Only the gage length (between 20 and 25 mm depending on the relative density) of the specimens was perforated. The tests were performed on the same testing machine.
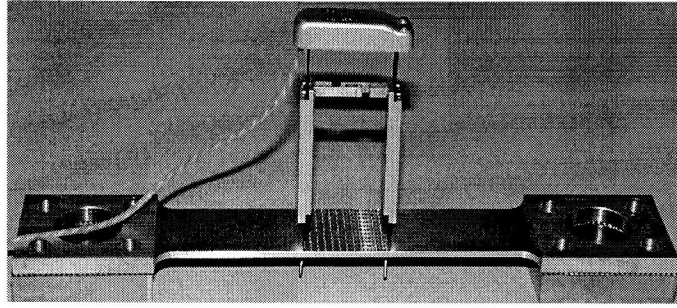

Figure 8: Tensile Specimen and Strain Measuring Instrument

For the evaluation of the tensile tests the same procedure was selected as with the compression tests. The results for the normalized stiffness and the yield stress are shown in Figure 9.
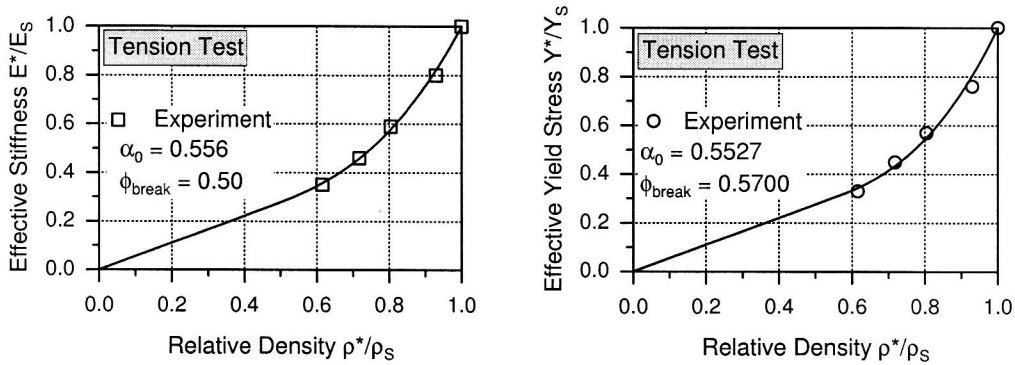

Figure 9: Results of Tension Tests

A comparison of the fit parameters α_0 and ϕ_{break} shows (cf. Table 2) a slight difference between the tension and compression experiments.

Test	Effective Stiffness		Effective Yield Stress	
	α_0	ϕ_{break}	α_0	ϕ_{break}
Compression	0.5278	0.4167	0.4623	0.4100
Tension	0.5560	0.5000	0.5527	0.5700

Table 2: Comparison of Fit Parameters

5 Finite Element Simulations

The nonlinear finite element program MSC/MARC was used for numerical simulation of the experiments. In view of the symmetric nature of the problem, it was necessary to discretize only one quarter of the specimen with appropriate boundary conditions for the finite element analysis (cf. Figure 10).

boundary conditions

$\rho^*/\rho_S = 0.9293$

Δl

$\rho^*/\rho_S = 0.8037$

$\rho^*/\rho_S = 0.7173$
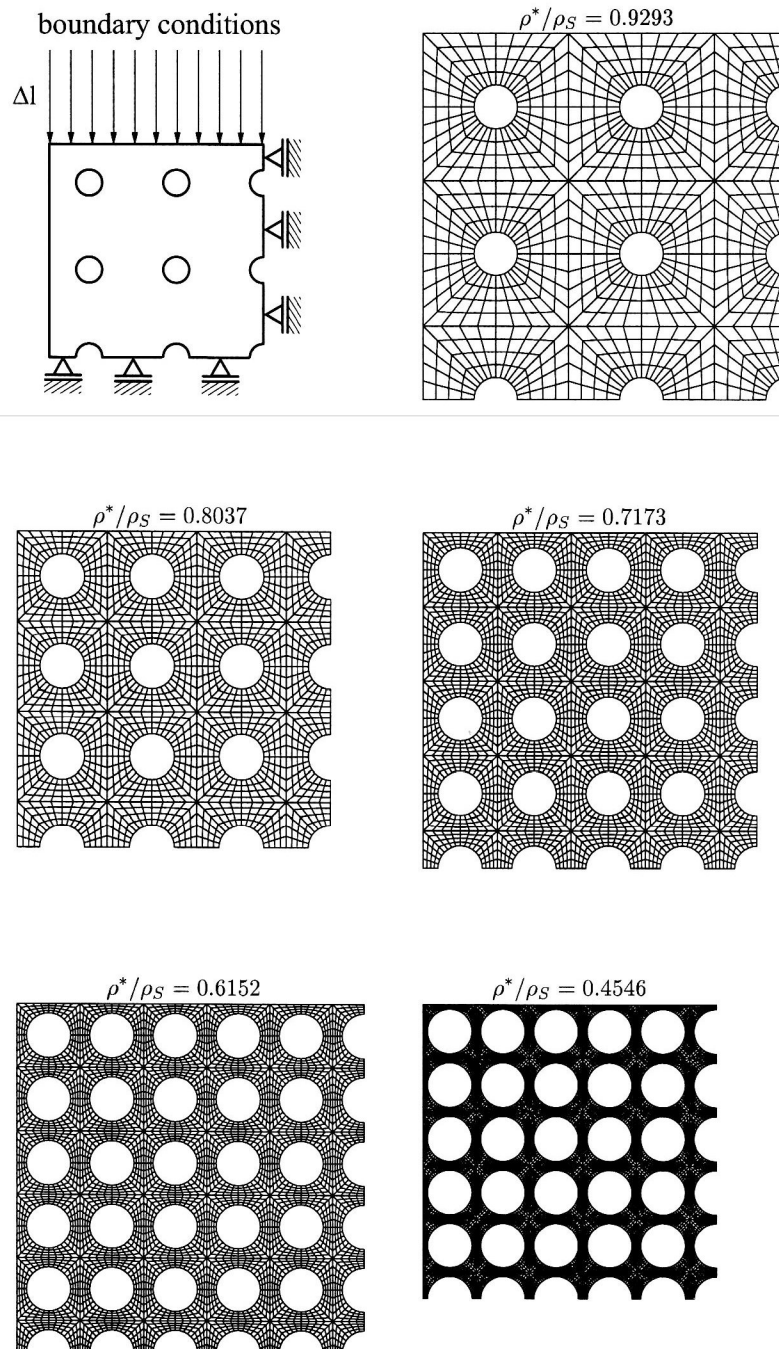
$\rho^*/\rho_S = 0.6152$

$\rho^*/\rho_S = 0.4546$

Figure 10: Finite Element Models

Eight-noded isoparametric solid elements were used and a number of computer runs was carried out to ensure the convergence of the selected mesh. Furthermore, the preliminary investigations showed that an inhibition of the transversal contraction in the load application area has a negligible influence on the results. Figure 10 shows the final meshes and the mesh data is summarized in Table 3.

The original unperforated material was assumed to be isotropic, work (isotropic) hardening and to obey the von Mises yield criterion with the associated (Prandtl-Reuss) flow rule. For determining the actual behaviour of the base material, uniaxial tension tests with (unnotched) rod specimens were performed

Relative Density ρ^*/ρ_S	0.9293	0.8037	0.7173	0.6152	0.4546
Number of Nodes	1874	3624	5946	8840	17640

Table 3: Mesh Density

and obtained average stress-strain curve was used for the FE input in terms of true stesses and logarithmic plastic strains. The following approach was adopted to obtain the average elastic and plastic properties for different relative densities. First, a prescribed longitudinal displacement was imposed incrementally upon the appropriate edge of the perforated plate. Second, the resulting average longitudinal stress was obtained for each computational step as the sum of corresponding forces at edge nodes divided by the initial cross-sectional area. The average strains were calculated from the imposed displacement divided by the initial length of the specimen. Third, a stress-strain plot was generated based on the numerical results. The average elastic and plastic characteristics were then determined according to the experimental procedure (cf. section 3). Specimens with small relative densities (< 0.5) can not be examined experimentally, since such specimens can not be manufactured due to too small pitch. However, a specimen with a relative density smaller than 0.5 could be simulated by means of the Finite Element Method. Figure 11 summarizes the results of the simulation. Comparisons between FEM and the experimental results (fit) reveal good agreement between the two. Furthermore, the simulation of the specimen with the smallest relative density confirms the progress of the material characteristics for small relative densities predicted through the experimental fit.
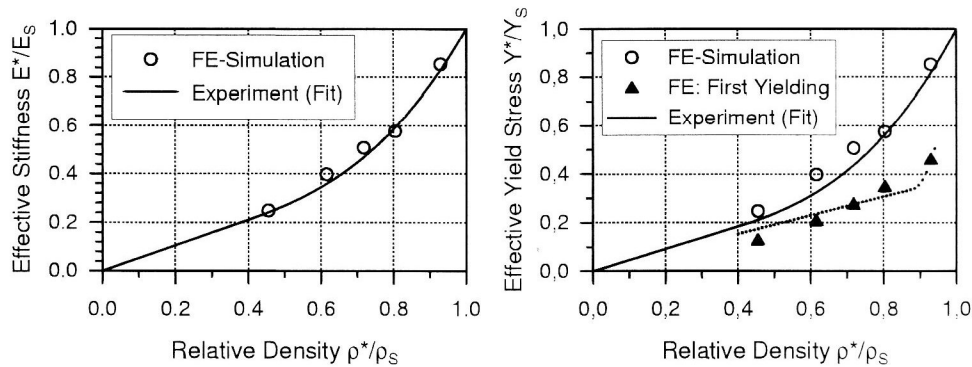

Figure 11: Results of Finite Element Simulation

It is important to note that the above calculated average yield stress is different from the inelastic deformation on the microscale. Therefore, the first yielding of a node occuring in the notch root of a drilled hole was recorded for every calculation. Figure 11 shows clearly that yielding on the microscale starts much earlier than the average values on the macroscale indicate. The application of the modified mixing rule for this initial yielding supplies the following parameters:

	α_0	ϕ_{break}
First Yielding	0.3889	0.8889

Table 4: Fit Parameters for First Yielding

6 Conclusions and Outlook

Both the elastic and the plastic characteristics of perforated aluminium-alloys under compression and tension load can be described in relation to its relative density. The experimental results can be simulated by means of the numeric calculations. Furthermore, it could be shown that first plastic processes on the microlevel can be observed far under the definitions on the macrolevel. In the future research work the perforated plates will be tested under pure shear load. These investigations will be realized with a modified Iosipescu shear test. The variation of the elastic modulus will be measured during unloading to investigate the damage evolution.

Literature

1. Ashby, M.F.; Evans, A.G.; Hutchinson, J.W.; Fleed, N.A.: Metal Foams, Butterworth-Heinemann, (2000).

2. Bailey, R.; Hicks, R.: Behaviour of perforated plates under plane stress, J. Mech. Eng. Science, 2, 2, (1960), 143 – 161.

3. Duncan, J.P.; Upfold, R.W.: Equivalent elastic properties of perforated bars and plates, J. Mech. Eng. Science, 5, 1, (1963), 53 – 65.

4. Gibson, L.J.; Ashby, M.F.: The mechanics of three-dimensional cellular materials, Proc. R. Soc. Lond., A 382, (1982), 43 – 59.

5. Gibson, L.J.; Ashby, M.F.: Cellular Solids - Structure and Properties, 2nd edition, Cambridge University Press, (1997).

6. Hashin, Z.: A variational approach to the theory of the elastic behaviour of multiphase materials, J. Mech. Phys. Solids, 11, (1963), 127 – 140.

7. Kuhn, G.; Winter, W.; Ströhla, S.: Festigkeit, Schädigung und Stoffgesetz zellularer Metalle unter mehrachsiger Beanspruchung, 1. Zwischenbericht zum DFG-Projekt Ku 360/15-1, Universität Erlangen-Nürnberg, Erlangen (2000).

8. Litewka, A.: Experimental study of the effective yield surface of perforated materials, Nuclear Engineering and Design, 57, (1980), 417 – 425.

9. Litewka, A.: Plasticity of perforated metal sheet with triangular penetration patterns, Res Mechanica Letters, 1, (1981), 253 – 259.

10. Markov, K.Z.: An anisotropic yield criterion for perforated plates, Res Mechanica Letters, 1, (1981), 315 – 318.

11. Meguid, S.A.; Kalamkarov, A.L.; Yao, J.; Zoudas, A.: Analytical, Numerical, and Experimental Studies of Effective Elastic Properties of Periodically Perforated Materials, J. Eng. Mat. Tech., 118, (1996), 43 – 48.

12. Öchsner, A.; Winter, W.; Kuhn, G.: Modified Voigt-Reuss mixing rules for cellular materials, Materials Science and Engineering A, submitted for publication.

13. Öchsner, A.; Winter, W.; Kuhn, G.: Damage and fracture of perforated aluminium alloys. Adv. Eng. Mat., 2, 7, (2000), 423 – 426.

14. Swan, C. C.; Kosaka, J.: Voigt-Reuss topology optimization for structures with linear elastic material behaviours, Int. J. Num. Meth. Eng., 40, (1997), 3033 – 3057.

Address: Dipl.-Ing. Andreas Öchsner, Dr.-Ing. Werner Winter and Prof. Dr.-Ing. habil. Günther Kuhn, Institute of Applied Mechanics, University of Erlangen-Nuremberg, Egerlandstraße 5, 91058 Erlangen, Germany, e-mail: oechsner@ltm.uni-erlangen.de